and for ribosomal protein L27 (RPL27, 5′-CCTCATGCCCACAAGGTACTC-3′ and 3′-TCGCTCCTCAAACTTGACC-5′) as an internal standard.

Total RNA was incubated with DNase I for 30 min and reverse transcription was performed with ReverTra Ace qPCR RT Kit (Toyobo). The relative amount of modulatory calcineurin interacting protein 1 (MCIP1) cDNA was quantified using in the same way as quantification of mtDNA copy number, using the PCR mixture contained 5 ng of the total cDNA, 12 pmol each of primers (5′-TTGGGAACTGTTGGTTGACA-3′ and 5′-ATGGCTACGGCATACTCCAC-3′ for MCIP1) in 30 μl.

In in vivo experiments, 8- to 10-week-old male TFAM overexpression mice and their littermates were used. Under anaesthesia with pentobarbital sodium (30 mg/g BW, i.p.), the hearts were excised and RNA was extracted with RNeasy tissue kit. After reverse transcription, the relative amount of cDNA was quantified using the PCR mixture contained 5 ng of the total cDNA, 12 pmol each of primers (5′-CCGTGTGGAATTGTCCTTCTC-3′ and 5′-GACCCCATGTGCAGAGAAAAC-3′ for MCIP1) in 30 μl. We used hypoxanthine guanine phosphoribosyl transferase (HPRT) gene as an internal standard (5′-CTGGTGAAAAG GACCTCTCG-3′ and 5′-AACTTGCGCTCATCTTAGGC-3′).

2.9. Nuclear translocation of NFAT

In order to assess nuclear translocation of NFAT, production and infection of recombinant adenovirus including green fluorescent protein (GFP)-fused N-terminal region of NFAT4 (we referred as just NFAT in this article) were performed as described previously (Fujii et al., 2005; Nishida et al., 2007). Cardiac myocytes were infected with the adenovirus at a multiplicity of infection of 300 for 60 h. After the stimulation for 30 min with angiotensin II (AngII, 100 nM, Sigma-Aldrich) or ET-1 (100 nM), cells were fixed by 10% formaldehyde (Sigma-Aldrich). The localization of GFP-NFAT was observed at an excitation wavelength of 488 nm with fluorescent microscopy (IX71, Olympus). More than 20 scenes were randomly scanned in each experiment and quantified the subcellular localization of GFP-NFAT using Photoshop (adobe systems).

2.10. Luciferase assays

NFAT-dependent luciferase activity and brain natriuretic peptide (BNP) promoter activity were measured as described previously (Fujii et al., 2005; Nishida et al., 2007, 2010). Cardiac myocytes were transiently co-transfected with 0.45 μg of pNFATLuc (Stratagene) and 0.05 μg of pRL-SV40 (Stratagene) control plasmid or with 0.3 μg of pBNP-Luc and 0.2 μg of pRL-SV40 using Fugene 6 (Roche Diagnostics) for 48 h followed by stimulation of AngII (100 nM) or ET-1 (100 nM). Luciferase activity was measured 6 h (for NFAT) or 24 h (for BNP) after the stimulation using dual luciferase reporter assay system (Promega) according to the manufacturer's protocol.

2.11. Measurement of mitochondrial [Ca^{2+}]

Mitochondrial [Ca^{2+}] was visualized using mitochondria-specific Ca^{2+} indicator, rhod-2/AM (Dojindo). Cardiac myocytes were loaded with 1 μM rhod-2/AM at 37 °C for 30 min. Then they were stimulated with AngII (100 nM) or ET-1 (100 nM), and the time course of fluorescence intensity was traced with a video image analysis system (Aquacosmos, Hamamatsu Photonics).

2.12. Measurement of hypertrophic response of cardiac myocytes

Hypertrophy of cells was assessed by a measurement of cell surface area and amount of actin filament, visualized by actin filament

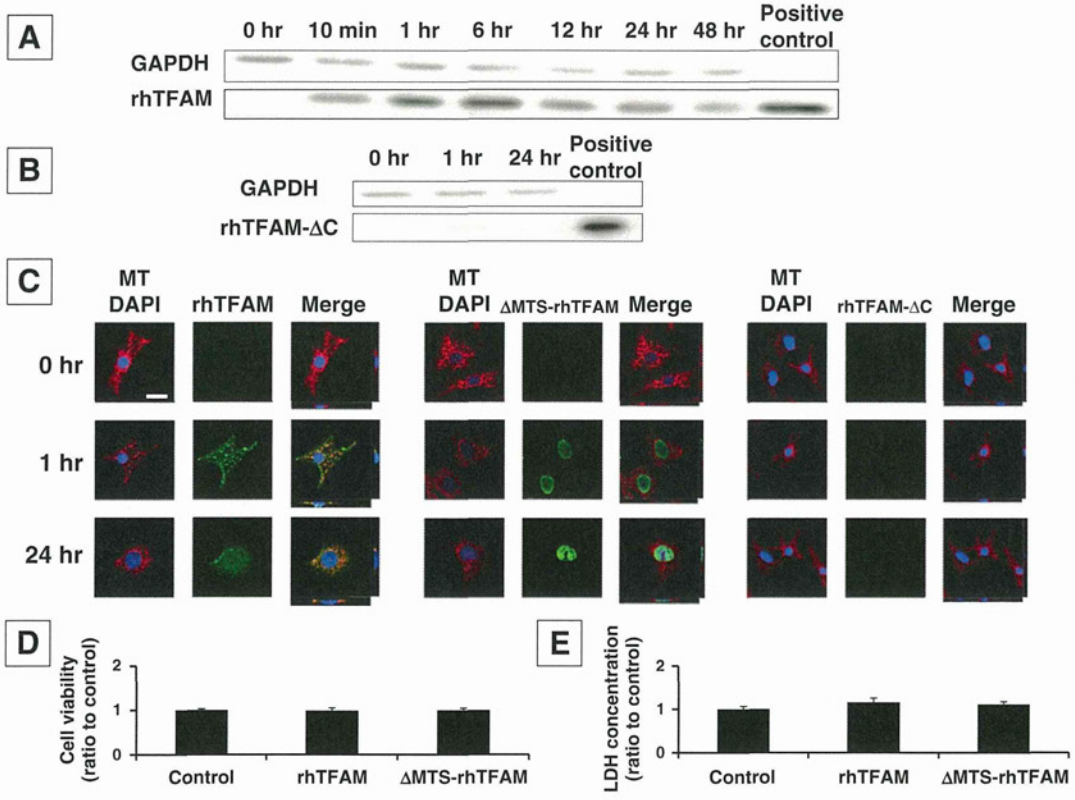

Fig. 2. The localization and cytotoxicity of rhTFAM proteins in cardiac myocytes. (A) Western blot analysis of myocytes treated with rhTFAM protein for 0–48 h. (B) Western blot analysis of myocytes treated with rhTFAM-ΔC protein for 0–24 h. (C) Confocal microscopic observations of myocytes treated with rhTFAM, ΔMTS-rhTFAM, or rhTFAM-ΔC. Red represents mitochondria (MT), green represents human TFAM (Alexa Fluor 488), and blue represents nucleus (DAPI). Scale bar = 20 μm. (D and E) The treatment with rhTFAM or ΔMTS-rhTFAM did not affect the cell viability (D) of myocytes and LDH concentration of the medium (E). Data are presented as ratio to control.

staining. Quantification of hypertrophy of myocytes was performed as previously described (Nishida et al., 2007, 2010). After AngII (100 nM) or ET-1 (100 nM) stimulation for 48 h, cells were fixed by 4% paraformaldehyde (nacalai tesque) and stained with Alexa Fluor 546 phalloidin (Invitrogen) for actin filaments visualization. Digital photographs were taken with confocal microscopy (FV-10i, Olympus) or Biozero Microscope (BZ-8000, Keyence), and the average values of the cell surface area and fluorescent intensity (more than 200 cells) were calculated using BZ-II Analyzer (Keyence).

2.13. Statistical analysis

Data are presented as mean ± standard error. Each experiment was repeated at least three times. Data were analyzed by a two-tailed Student's *t* test or analysis of variance followed by the Tukey post-hoc test with significance imparted at P values of <0.05.

3. Results

3.1. rhTFAM was recruited into the mitochondria of cardiac myocytes

We synthesized rhTFAM protein and investigated its recruitment into cardiac myocytes since we expected it as a new therapeutic modality. rhTFAM (100 nM) was just added to the culture medium of myocytes. rhTFAM protein rapidly entered into cultured rat neonatal ventricular myocytes within 10 min of the treatment, and remained in the cells even at 48 h (Fig. 2A). In contrast, rhTFAM-ΔC rarely entered into the cells (Fig. 2B). Confocal microscopy with z-scale analysis revealed that exogenously added rhTFAM localized both in the cytoplasm and mitochondria, whereas ΔMTS-rhTFAM was recruited mostly into the nucleus (Fig. 2C), both for 1 and 24 h treatment. These results suggested that MTS played an important role in determining the localization of recombinant TFAM in myocytes. We confirmed that rhTFAM-ΔC was not recruited into the cells (Fig. 2C), suggesting that some sequence in C-terminal tail of TFAM was important for the recruitment of this protein.

Moreover, ΔMTS-rhTFAM and rhTFAM had no significant cytotoxicity in cardiac myocytes at least at the concentration which we used in these experiments (100 nM), since cell viability did not alter (Fig. 2D) and LDH concentration in culture medium did not increase (Fig. 2E) after the treatment with ΔMTS-rhTFAM or rhTFAM.

3.2. rhTFAM increased mtDNA copy number and mtDNA-encoded proteins

In order to determine whether this recombinant protein functions in cardiac myocytes, we performed characterization of mitochondria after the treatment with rhTFAM. rhTFAM treatment increased mtDNA copy number dose-dependently (0–100 nM) with a maximum increase of approximately two-fold at 12 h, whereas mtDNA copy number was not affected by the treatment with ΔMTS-rhTFAM (Fig. 3A). We confirmed these results by two different PCR primer sets for mtDNA quantification and concluded that rhTFAM recruited into mitochondria functioned and directly increased mtDNA copy number. Using extract from empty vector, we ruled out the possibility that products other than rhTFAM from competent cells increased mtDNA contents (Fig. 3B). The treatment with rhTFAM or ΔMTS-rhTFAM (100 nM) for 24 h did not affect the morphology and the number of mitochondria significantly in cardiac myocytes (Fig. 3C).

To rule out the possibility that the recruitment and function of rhTFAM are the specific property of cardiac myocytes, we used another type of cell, RAW 264.7, to examine whether it also allows rhTFAM to enter into the cells. We found both rhTFAM and ΔMTS-rhTFAM were successfully recruited into RAW 264.7 cells (Fig. 4A and B). Subsequently, rhTFAM functioned to increase mtDNA copy number, but ΔMTS-rhTFAM did not (Fig. 4C). The recruitment and function of rhTFAM were similar to cardiac myocytes, suggesting that they were not unique properties of myocytes, but those of this specific protein.

In order to characterize the change of mitochondrial features by rhTFAM, we investigated the expression of mitochondrial electron transport complex proteins in cardiac myocytes. rhTFAM (100 nM)

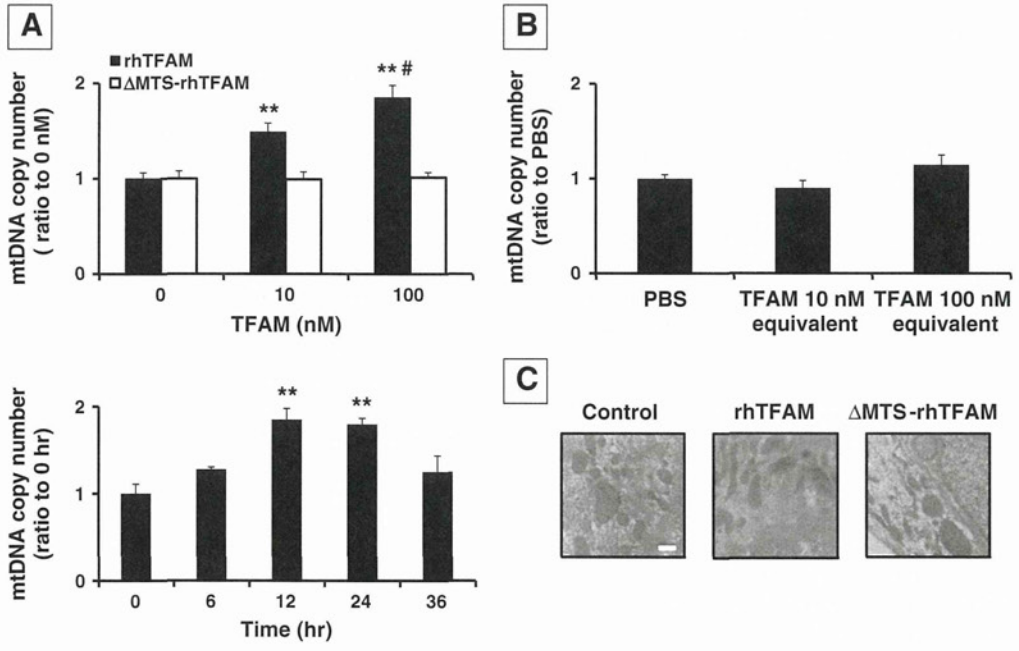

Fig. 3. The effects of rhTFAM on mitochondrial characteristics. (A) mtDNA copy number in myocytes treated with rhTFAM or ΔMTS-rhTFAM (0–100 nM) for 12 h, and rhTFAM (100 nM) for 0–36 h, quantified by real-time PCR relative to nucleus genome (ATIII gene). Data are presented as ratio to 0 nM or 0 h. **: $P<0.01$ vs. 0 nM or 0 h, #: $P<0.05$ vs. 10 nM. (B) mtDNA copy number of myocytes after the treatment with the product from empty vector. Myocytes were treated with the product from the empty vector by the equivalent volume of rhTFAM 10 or 100 nM, and mtDNA copy number was quantified. Data are shown as a ratio to buffer control (PBS). Values are mean ± SEM. (C) rhTFAM or ΔMTS-rhTFAM did not affect the morphology and number of mitochondria in cardiac myocytes, observed by TEM. Scale bar = 1 μm.

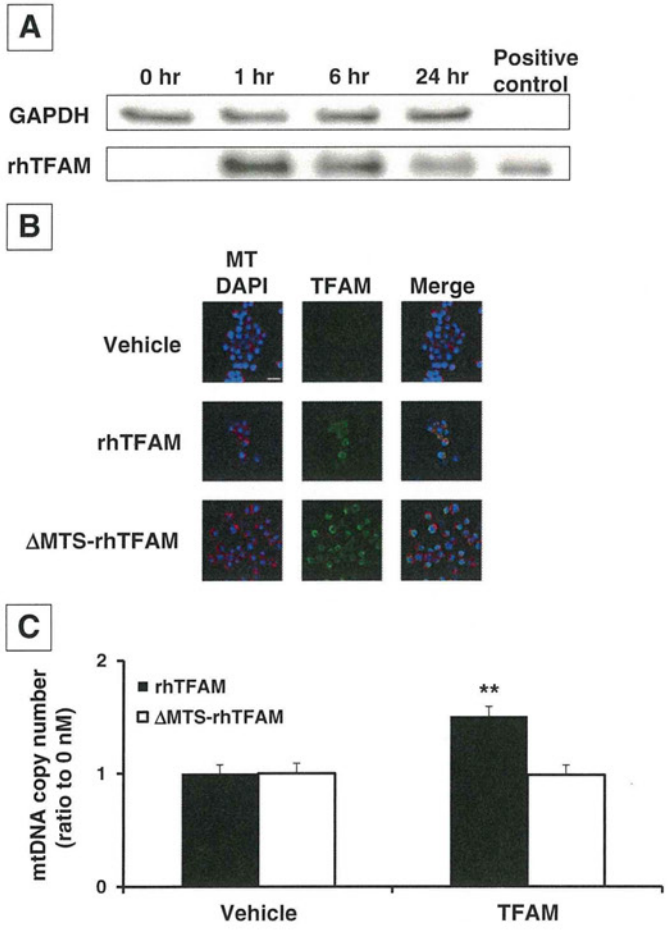

Fig. 4. The recruitment and function of rhTFAM on RAW 264.7 cells. (A) Western blot analysis of RAW 264.7 cells treated with rhTFAM protein for 0–24 h. (B) Confocal microscopic observations of RAW 264.7 cells treated with rhTFAM or ΔMTS-rhTFAM. Red represents mitochondria (MT), green represents human TFAM (Alexa Fluor 488), and blue represents nucleus (DAPI). Scale bar = 10 μm. (C) mtDNA copy number in RAW 264.7 cells treated with rhTFAM or ΔMTS-rhTFAM (50 nM) for 12 h, quantified by real-time PCR relative to nucleus genome (RPL27 gene). Data are presented as ratio to vehicle. **: $P<0.01$ vs. vehicle.

increased mtDNA-encoded COX I and COX III protein expression, which is a component of mitochondrial electron transport complex IV (Fig. 5A and B). In contrast, there were no increase of nuclear DNA-encoded NDUFA9 (complex I component) and SDHA (complex II component) protein contents (Fig. 5C and D). These results suggested that rhTFAM increased mtDNA copy number and subsequently increased mtDNA-encoded, but not nuclear DNA-encoded, mitochondrial proteins.

3.3. rhTFAM inhibited nuclear translocation of NFAT, NFAT transcriptional activity, and NFAT-dependent gene expression

Since overexpression of TFAM ameliorated post-MI remodeling in vivo, we expected rhTFAM also attenuated pathological hypertrophy and remodeling signals. The calcineurin/NFAT signaling pathway is a crucial signal that promotes pathological cardiac hypertrophy, both in vitro and in vivo (McKinsey and Kass, 2007; Molkentin, 2004; Vega et al., 2003). Dephosphorylation of NFAT by calcineurin, a Ca^{2+}-dependent serine/threonine phosphatase, induces cytosol-to-nucleus translocation, and NFAT functions as a transcriptional factor that activates many prohypertrophic genes. Furthermore, previous reports have suggested that the inhibition of NFAT signaling attenuated cardiac hypertrophy and failure (Sakata et al., 2000; van Rooij et al., 2004). We hypothesized that rhTFAM could also inhibit NFAT activation. We stimulated cardiac myocytes with AngII or ET-1, which are the major neurohumoral factors of pathological cardiac hypertrophy. First we investigated whether rhTFAM attenuated AngII- or ET-1-induced NFAT nuclear translocation using recombinant adenovirus encoding GFP-NFAT. The pretreatment with rhTFAM (100 nM) significantly inhibited AngII (100 nM)- or ET-1 (100 nM)-induced nuclear translocation of GFP-NFAT, whereas the pretreatment with ΔMTS-rhTFAM (100 nM) had no effect (Fig. 6A and B). This result suggested that recombinant TFAM recruited in mitochondria inhibited AngII- or ET-1-induced NFAT activation. Moreover, NFAT transcriptional activity as assessed by luciferase assay increased approximately 2.5-fold by stimulation with AngII (100 nM) or ET-1 (100 nM), and these increases were totally inhibited by the pretreatment with rhTFAM (10 nM) (Fig. 6C). The promoter activity of BNP gene, a NFAT-target gene widely used as marker of pathological cardiac hypertrophy, was also suppressed by rhTFAM (10 nM) (Fig. 6D). The expression of MCIP1 gene is also regulated by NFAT, and is used as a reporter gene of NFAT (Jin et al., 2010). MCIP1 mRNA expression was inhibited by the treatment with rhTFAM at baseline, just like TFAM-overexpression mice (Fig. 6E and F). These results confirmed that rhTFAM attenuated AngII- or ET-1-induced NFAT activation in cardiac myocytes.

We also investigated whether rhTFAM modulates MAPK p44/42 (ERK 1/2), another important pathway that induces cardiac hypertrophy (Aoki et al., 2000; McKinsey and Kass, 2007). The pretreatment with rhTFAM (100 nM) had no effect on ET-1 (100 nM)-induced MAPK p44/42 phosphorylation level (Fig. 7), suggesting that rhTFAM attenuates hypertrophy independent of MAPK signaling.

Since NFAT is regulated by the frequency of Ca^{2+} oscillation, we investigated the effect of rhTFAM on Ca^{2+} release from mitochondria. Stimulation with AngII (100 nM) or ET-1 (100 nM) decreased mitochondrial $[Ca^{2+}]$ in cardiac myocytes, and rhTFAM (10 nM) significantly suppressed these decrease (Fig. 8). This result suggested that rhTFAM suppressed AngII- or ET-1-induced Ca^{2+} release from mitochondria to cytoplasm.

3.4. rhTFAM attenuated pathological hypertrophy of cardiac myocytes

Finally we examined whether rhTFAM subsequently attenuates hypertrophic response of myocytes. The treatment with rhTFAM (10 nM) significantly reduced the hypertrophic reactions induced by the stimulation with AngII (100 nM) or ET-1 (100 nM) for 48 h (Fig. 9A–C). We concluded that rhTFAM attenuates AngII- or ET-1-induced hypertrophy of cardiac myocytes.

4. Discussion

In our previous report we showed that, after MI, the overexpression of TFAM attenuated the decrease of mtDNA copy number, ameliorated pathological hypertrophy and improved survival rate dramatically (Ikeuchi et al., 2005). Thus from the clinical point of view, our next interest was to find the strategy to increase TFAM or mtDNA copy number efficiently. Accordingly, this report has mainly two novel findings. First, this is the first report showing that rhTFAM protein is successfully recruited into mitochondria of cardiac myocytes, and functions to increase mtDNA copy number. The other finding is that rhTFAM inhibits NFAT signaling and consequently attenuates morphological remodeling of cardiac myocytes. These results will enable novel new strategy to increase mtDNA copy number and attenuate pathological cardiac hypertrophy.

4.1. The recruitment of rhTFAM into cardiac myocytes

Previously it has been reported that recombinant TFAM with protein transduction domain was entered into cultured cells (Iyer et al., 2009). This study is the first report that rhTFAM which has the almost

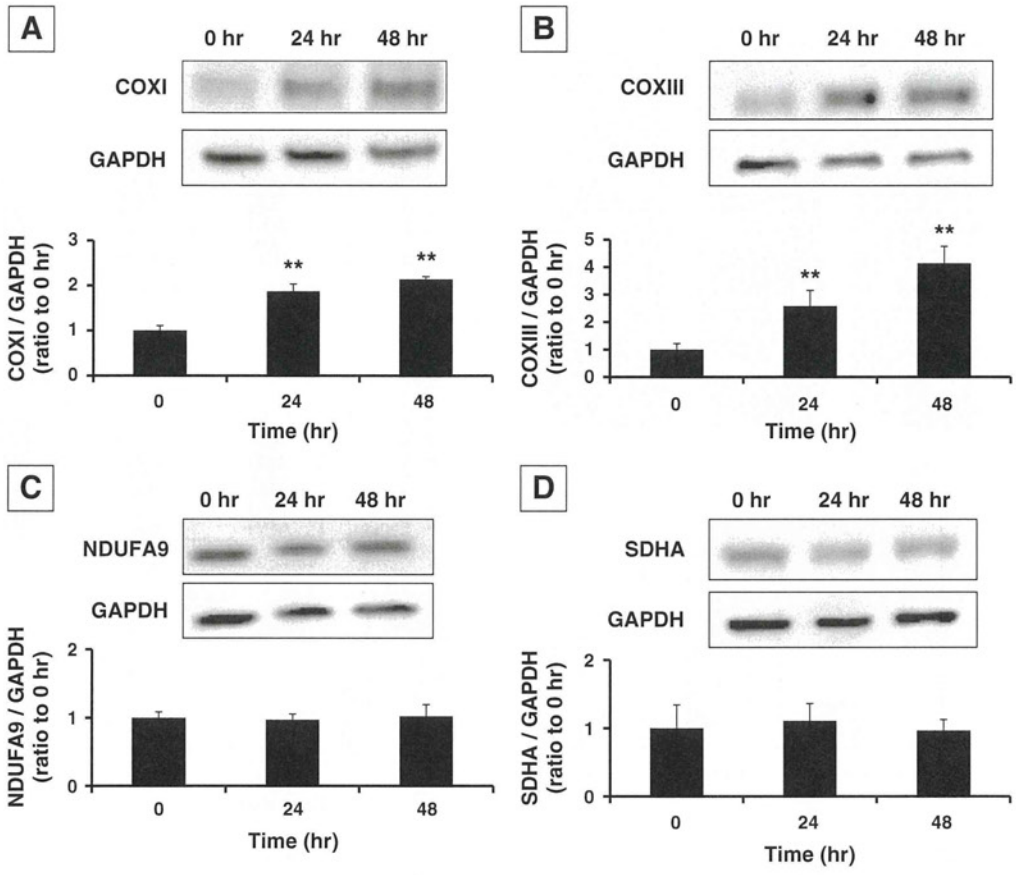

Fig. 5. The effects of rhTFAM on mitochondrial electron transport complex proteins. (A–D) The protein expression of COX I (A), COX III (B), NDUFA9 (C), and SDHA (D), 0–48 h after the treatment with rhTFAM. Data are presented as ratio to 0 h. **: $P<0.01$ vs. 0 h. Values are mean ± SEM.

identical amino acid sequence with native human TFAM can be successfully recruited into cardiac myocytes. Our result that rhTFAM-ΔC did not recruit into cells suggests that C-terminal tail of TFAM is responsible for this interesting property. Furthermore, we confirmed the recruitment and function of rhTFAM are independent of the cell types. The mechanism of its recruitment into cardiac myocytes remains unknown. Our data that rhTFAM entered into cells as early as 10 min, which was not inhibited in low temperature nor endocytosis inhibitors (data not shown), provides possibility that rhTFAM recruited into cytosol by a receptor-mediated pathway. Further investigations for the identification of the pathways for the recruitment of recombinant TFAM into the cells are necessary.

4.2. The effect of rhTFAM on mitochondrial characteristics

rhTFAM increased mtDNA copy number in myocytes (Fig. 3A) in a dose-dependent manner. Other than functioning as a transcription factor, endogenous TFAM regulates the amount of mtDNA by stabilizing mtDNA by forming a nucleoid structure (Kang et al., 2007). Considering the previous finding that the amount of mtDNA changes corresponding to the amount of TFAM, our results suggest that exogenously administered rhTFAM functioned similarly just like endogenous TFAM (Kanki et al., 2004). Furthermore, since ΔMTS-rhTFAM entered into myocytes but did not increase mtDNA copy number, it is likely that rhTFAM that entered mitochondria increased mtDNA copies. In this study, the mtDNA copy number peaked at 12 to 24 h after the rhTFAM treatment, and declined gradually thereafter. A single treatment with rhTFAM in myocytes prior to AngII or ET-1 stimulation successfully ameliorated pathological remodeling signals and subsequent pathological hypertrophy.

rhTFAM increased mtDNA-encoded, but not nuclear-encoded, mitochondrial proteins (Fig. 5). Probably it will be because of the increased mtDNA copy number, which is consistent with other's previous report that recombinant TFAM with protein transduction domain increased mitochondrial electron transport function and ATP synthesis in cultured cells (Thomas et al., 2011).

4.3. The effect of rhTFAM on NFAT signaling and pathological hypertrophy

The treatment with rhTFAM inhibited NFAT signaling in cardiac myocytes, and subsequent gene expression of MCIP1, which is a downstream of NFAT signaling, as well as in TFAM-overexpression mice hearts (Fig. 6E and F). The mechanism how rhTFAM inhibited AngII or ET-1-induced NFAT activation and hypertrophic response remains unknown. We need further investigation about the precise mechanism. Since mitochondria is known to participate in intracellular Ca^{2+} homeostasis via several Ca^{2+} uptake and release pathways (Bernardi, 1999), we speculated that rhTFAM inhibited Ca^{2+}/calcineurin-NFAT signaling by modulating $[Ca^{2+}]$. In fact, AngII or ET-1 induced the decrease of mitochondrial $[Ca^{2+}]$, suggesting the increase of Ca^{2+} release from mitochondria to cytoplasm, and rhTFAM inhibited AngII or ET-1-induced decrease of mitochondrial $[Ca^{2+}]$ (Fig. 8). However, the mechanism how rhTFAM inhibited AngII or ET-1-induced mitochondrial Ca^{2+} release still remains unknown. AngII is known to increase mitochondrial ROS in cardiac myocytes (Dai et al., 2011a, 2011b), and increased mitochondrial ROS is associated with mitochondrial Ca^{2+} release from mitochondria to cytoplasm (Kalivendi et al., 2005). rhTFAM inhibited superoxide production induced by rotenone, a complex I inhibitor, in cardiac myocytes (data not shown). Accordingly, the impact of rhTFAM on mitochondrial $[Ca^{2+}]$ might be associated with the inhibition of excessive mitochondrial ROS generation.

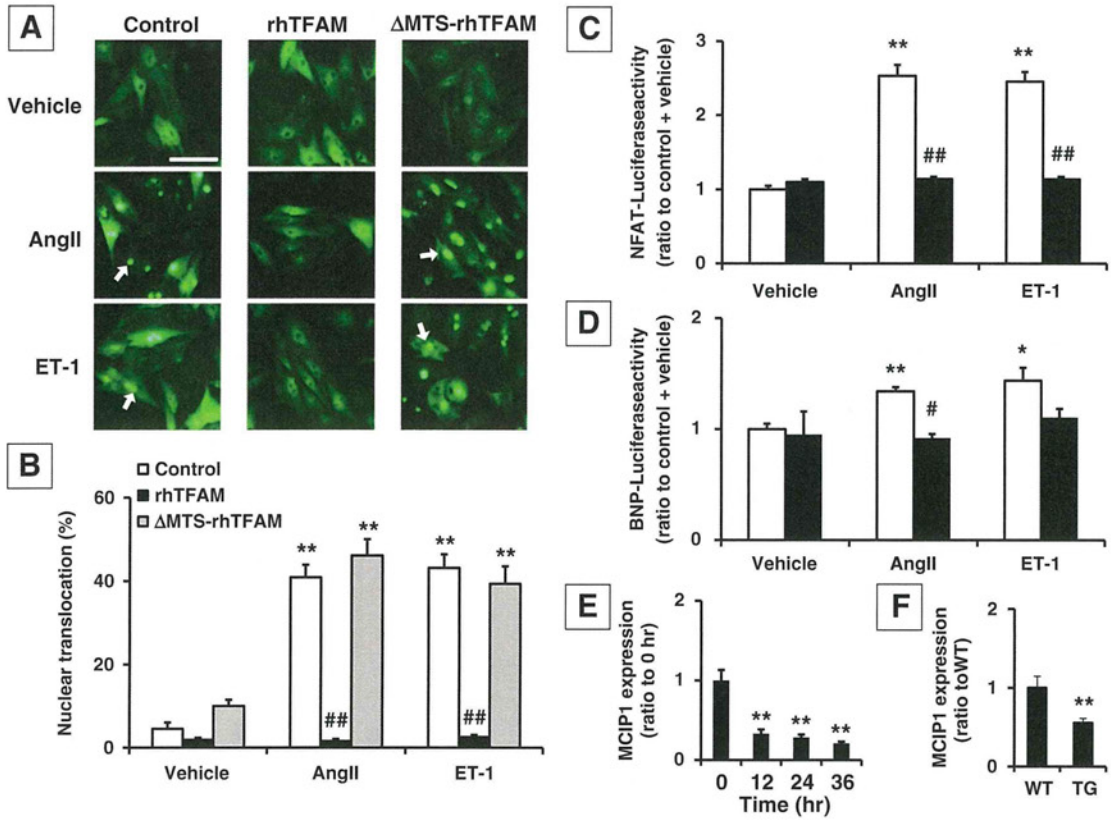

Fig. 6. The effects of rhTFAM on NFAT signaling. (A) The localization of GFP-NFAT protein in cardiac myocytes after the stimulation with AngII or ET-1. Arrows show GFP-NFAT translocated to nucleus. Scale bar = 50 μm. (B) rhTFAM significantly reduced the nuclear translocation rate of GFP-NFAT, whereas ΔMTS-rhTFAM had no effect on this translocation. (C and D) NFAT-luciferase activity (C) and BNP-luciferase activity (D) of myocytes stimulated with AngII or ET-1. NFAT- and BNP-luciferase activities were quantified as ratios to SV40 luciferase activity. Data are presented as ratio to control + vehicle. **: $P<0.01$, *: $P<0.05$ vs. control + vehicle; ##: $P<0.01$, #: $P<0.05$ vs. control. (E) MCIP1 mRNA expression in cardiac myocytes, 0–36 h after the treatment with rhTFAM. Data are presented as ratio to 0 h. **: $P<0.01$ vs. 0 h. (F) Cardiac MCIP1 mRNA expression of TFAM-overexpression mice and wild type littermates ($n=5$). WT means wild type mice, and TG means TFAM-overexpression mice. **: $P<0.01$ vs. WT. Values are mean ± SEM.

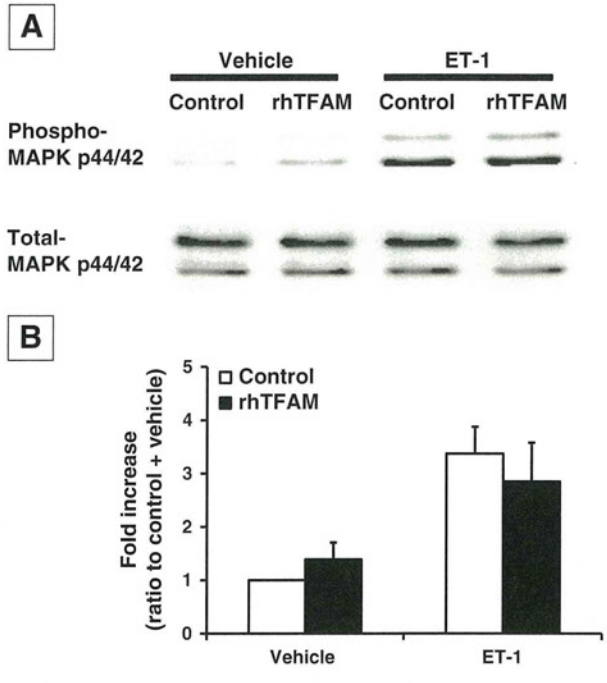

Fig. 7. The effects of rhTFAM on phosphorylation of MAPK p44/42. (A) Western blot analysis of myocytes probed with phospho-specific antibody and then reprobed for total protein. (B) The quantification of the ratio of phospho- to total-MAPK p44/42. The values were normalized to control + vehicle, and the data are shown as ratio to control + vehicle. Values are mean ± SEM.

NFAT signaling participates in pathological but not in physiological hypertrophy (Wilkins et al., 2004). Although hypertrophy has been traditionally viewed as a necessary first response to pathological stress but only later exacerbates disease, recent data suggest that hypertrophy in response to pathological stress may never be truly adaptive, and clinical studies support benefits from its inhibition (Frey et al., 2004; Gardin and Lauer, 2004; McKinsey and Kass, 2007). Moreover, the inhibition of NFAT signaling is reported to attenuate cardiac hypertrophy and failure (Sakata et al., 2000; van Rooij et al., 2004). Taken together, we believe that inhibiting NFAT signaling using rhTFAM can prevent cardiac hypertrophy and lead to the prevention of heart failure. We need further investigation, especially in vivo experiments, to confirm rhTFAM inhibits pathological cardiac hypertrophy and failure.

A possibility still exist that rhTFAM affected on other pathways besides NFAT signaling and subsequently inhibited AngII- or ET-1-induced hypertrophy of cardiac myocytes. However, we conclude in this study that exogenous rhTFAM have potential to increase mtDNA and inhibit pathological NFAT signaling in myocytes. Further elucidation of the precise mechanisms that TFAM functions in failing myocardium will be necessary.

5. Clinical implications

We propose in this report extreme novel findings that exogenously administered rhTFAM increased mtDNA copy number and attenuated pathological hypertrophy of cardiac myocytes. Thus rhTFAM could be a novel clinical strategy to increase mtDNA copy number and subsequently inhibit cardiac hypertrophy and failure. Further investigations of rhTFAM are anticipated.

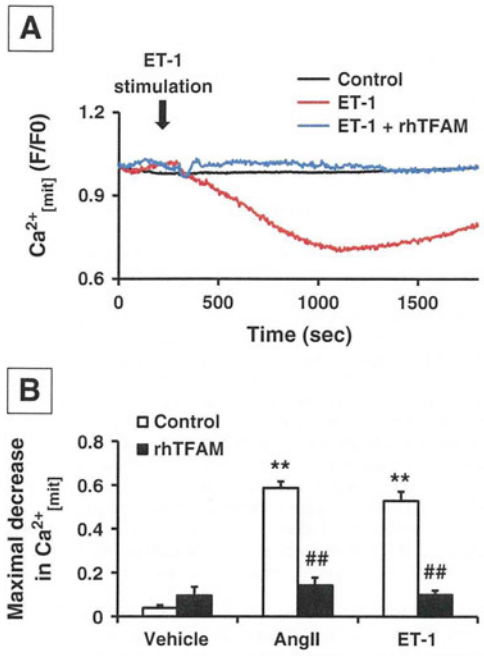

Fig. 8. The effects of rhTFAM on mitochondrial [Ca^{2+}]. (A) Representative trace of mitochondrial [Ca^{2+}] after the stimulation with ET-1, visualized using rhod-2. (B) rhTFAM significantly attenuated AngII- or ET-1-induced decrease of mitochondrial [Ca^{2+}]. **: $P<0.01$ vs. control + vehicle, ##: $P<0.01$ vs. control. Values are mean ± SEM.

Funding

This work was supported by Grant-in-Aid for Scientific Research (S) (23220013) and for Scientific Research (C) (23591084) from the Japan Society for the Promotion of Science.

Disclosures

None.

Acknowledgements

We thank Ms. Michiyo Tanaka for technical assistant. We appreciate the technical support from the Research Support Center, Graduate School of Medical Sciences, Kyushu University.

References

Alam, T.I., Kanki, T., Muta, T., Ukaji, K., Abe, Y., Nakayama, H., Takio, K., Hamasaki, N., Kang, D., 2003. Human mitochondrial DNA is packaged with TFAM. Nucleic Acids Res. 31, 1640–1645.

Aoki, H., Richmond, M., Izumo, S., Sadoshima, J., 2000. Specific role of the extracellular signal-regulated kinase pathway in angiotensin II-induced cardiac hypertrophy in vitro. Biochem. J. 347 (Pt 1), 275–284.

Bernardi, P., 1999. Mitochondrial transport of cations: channels, exchangers, and permeability transition. Physiol. Rev. 79, 1127–1155.

Dai, D.F., Chen, T., Szeto, H., Nieves-Cintron, M., Kutyavin, V., Santana, L.F., Rabinovitch, P.S., 2011a. Mitochondrial targeted antioxidant peptide ameliorates hypertensive cardiomyopathy. J. Am. Coll. Cardiol. 58, 73–82.

Dai, D.F., Johnson, S.C., Villarin, J.J., Chin, M.T., Nieves-Cintron, M., Chen, T., Marcinek, D.J., Dorn II, G.W., Kang, Y.J., Prolla, T.A., Santana, L.F., Rabinovitch, P.S., 2011b. Mitochondrial oxidative stress mediates angiotensin II-induced cardiac hypertrophy and Galphaq overexpression-induced heart failure. Circ. Res. 108, 837–846.

Frey, N., Katus, H.A., Olson, E.N., Hill, J.A., 2004. Hypertrophy of the heart: a new therapeutic target? Circulation 109, 1580–1589.

Fujii, T., Onohara, N., Maruyama, Y., Tanabe, S., Kobayashi, H., Fukutomi, M., Nagamatsu, Y., Nishihara, N., Inoue, R., Sumimoto, H., Shibasaki, F., Nagao, T., Nishida, M., Kurose, H., 2005. Galpha12/13-mediated production of reactive oxygen species is critical for angiotensin receptor-induced NFAT activation in cardiac fibroblasts. J. Biol. Chem. 280, 23041–23047.

Gardin, J.M., Lauer, M.S., 2004. Left ventricular hypertrophy: the next treatable, silent killer? JAMA 292, 2396–2398.

Garnier, A., Fortin, D., Delomenie, C., Momken, I., Veksler, V., Ventura-Clapier, R., 2003. Depressed mitochondrial transcription factors and oxidative capacity in rat failing cardiac and skeletal muscles. J. Physiol. 551, 491–501.

Hayashi, Y., Yoshida, M., Yamato, M., Ide, T., Wu, Z., Ochi-Shindou, M., Kanki, T., Kang, D., Sunagawa, K., Tsutsui, H., Nakanishi, H., 2008. Reverse of age-dependent

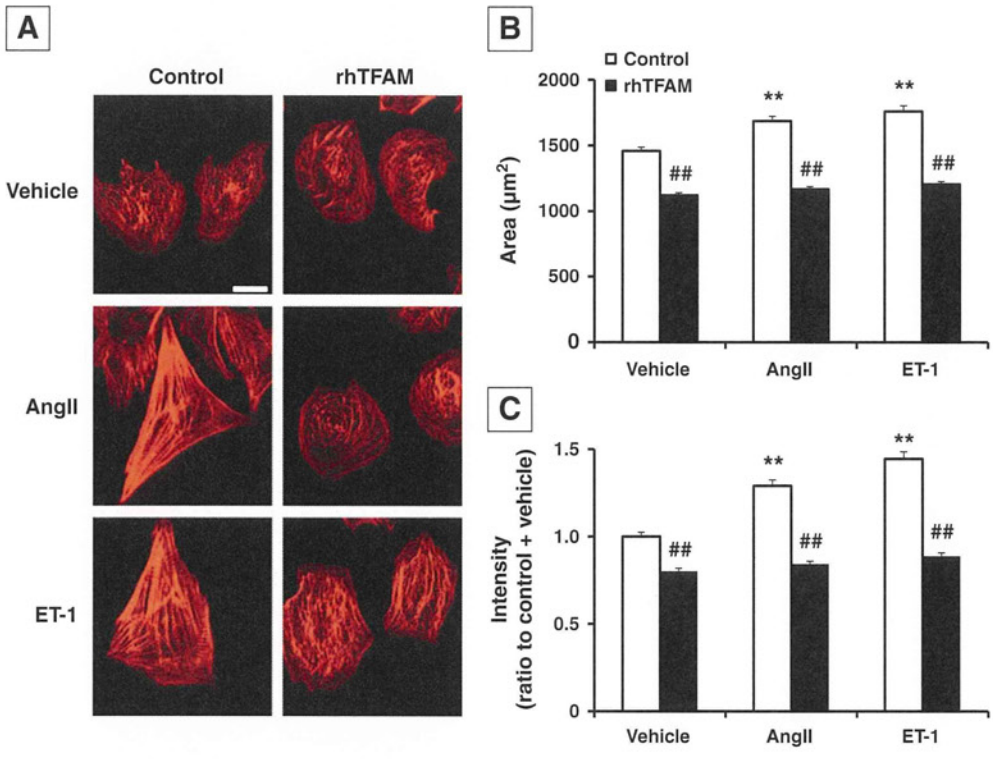

Fig. 9. Morphological remodeling of cardiac myocytes stimulated with AngII or ET-1. (A) Representative photomicrographs of AngII- or ET-1-stimulated myocytes immunostained using phalloidin. Scale bar = 20 μm. (B and C) Mean cell surface area (B) and fluorescent intensity (C) of 200–250 cells. **: $P<0.01$ vs. control + vehicle, ##: $P<0.01$ vs. control. Values are mean ± SEM.

memory impairment and mitochondrial DNA damage in microglia by an overexpression of human mitochondrial transcription factor a in mice. J. Neurosci. 28, 8624–8634.
Ide, T., Tsutsui, H., Hayashidani, S., Kang, D., Suematsu, N., Nakamura, K., Utsumi, H., Hamasaki, N., Takeshita, A., 2001. Mitochondrial DNA damage and dysfunction associated with oxidative stress in failing hearts after myocardial infarction. Circ. Res. 88, 529–535.
Ikeuchi, M., Matsusaka, H., Kang, D., Matsushima, S., Ide, T., Kubota, T., Fujiwara, T., Hamasaki, N., Takeshita, A., Sunagawa, K., Tsutsui, H., 2005. Overexpression of mitochondrial transcription factor a ameliorates mitochondrial deficiencies and cardiac failure after myocardial infarction. Circulation 112, 683–690.
Iyer, S., Thomas, R.R., Portell, F.R., Dunham, L.D., Quigley, C.K., Bennett Jr., J.P., 2009. Recombinant mitochondrial transcription factor A with N-terminal mitochondrial transduction domain increases respiration and mitochondrial gene expression. Mitochondrion 9, 196–203.
Jin, H., Hadri, L., Palomeque, J., Morel, C., Karakikes, I., Kaprielian, R., Hajjar, R., Lebeche, D., 2010. KChIP2 attenuates cardiac hypertrophy through regulation of Ito and intracellular calcium signaling. J. Mol. Cell. Cardiol. 48, 1169–1179.
Kalivendi, S.V., Konorev, E.A., Cunningham, S., Vanamala, S.K., Kaji, E.H., Joseph, J., Kalyanaraman, B., 2005. Doxorubicin activates nuclear factor of activated T-lymphocytes and Fas ligand transcription: role of mitochondrial reactive oxygen species and calcium. Biochem. J. 389, 527–539.
Kang, D., Kim, S.H., Hamasaki, N., 2007. Mitochondrial transcription factor A (TFAM): roles in maintenance of mtDNA and cellular functions. Mitochondrion 7, 39–44.
Kanki, T., Ohgaki, K., Gaspari, M., Gustafsson, C.M., Fukuoh, A., Sasaki, N., Hamasaki, N., Kang, D., 2004. Architectural role of mitochondrial transcription factor A in maintenance of human mitochondrial DNA. Mol. Cell. Biol. 24, 9823–9834.
Karamanlidis, G., Nascimben, L., Couper, G.S., Shekar, P.S., del Monte, F., Tian, R., 2010. Defective DNA replication impairs mitochondrial biogenesis in human failing hearts. Circ. Res. 106, 1541–1548.
Lagouge, M., Argmann, C., Gerhart-Hines, Z., Meziane, H., Lerin, C., Daussin, F., Messadeq, N., Milne, J., Lambert, P., Elliott, P., Geny, B., Laakso, M., Puigserver, P., Auwerx, J., 2006. Resveratrol improves mitochondrial function and protects against metabolic disease by activating SIRT1 and PGC-1alpha. Cell 127, 1109–1122.
Larsson, N.G., Wang, J., Wilhelmsson, H., Oldfors, A., Rustin, P., Lewandoski, M., Barsh, G.S., Clayton, D.A., 1998. Mitochondrial transcription factor A is necessary for mtDNA maintenance and embryogenesis in mice. Nat. Genet. 18, 231–236.
Li, H., Wang, J., Wilhelmsson, H., Hansson, A., Thoren, P., Duffy, J., Rustin, P., Larsson, N.G., 2000. Genetic modification of survival in tissue-specific knockout mice with mitochondrial cardiomyopathy. Proc. Natl. Acad. Sci. U. S. A. 97, 3467–3472.
McKinsey, T.A., Kass, D.A., 2007. Small-molecule therapies for cardiac hypertrophy: moving beneath the cell surface. Nat. Rev. Drug Discov. 6, 617–635.
Molkentin, J.D., 2004. Calcineurin-NFAT signaling regulates the cardiac hypertrophic response in coordination with the MAPKs. Cardiovasc. Res. 63, 467–475.
Nishida, M., Onohara, N., Sato, Y., Suda, R., Ogushi, M., Tanabe, S., Inoue, R., Mori, Y., Kurose, H., 2007. Galpha12/13-mediated up-regulation of TRPC6 negatively regulates endothelin-1-induced cardiac myofibroblast formation and collagen synthesis through nuclear factor of activated T cells activation. J. Biol. Chem. 282, 23117–23128.
Nishida, M., Watanabe, K., Sato, Y., Nakaya, M., Kitajima, N., Ide, T., Inoue, R., Kurose, H., 2010. Phosphorylation of TRPC6 channels at Thr69 is required for anti-hypertrophic effects of phosphodiesterase 5 inhibition. J. Biol. Chem. 285, 13244–13253.
Ohgaki, K., Kanki, T., Fukuoh, A., Kurisaki, H., Aoki, Y., Ikeuchi, M., Kim, S.H., Hamasaki, N., Kang, D., 2007. The C-terminal tail of mitochondrial transcription factor a markedly strengthens its general binding to DNA. J. Biochem. 141, 201–211.
Parisi, M.A., Clayton, D.A., 1991. Similarity of human mitochondrial transcription factor 1 to high mobility group proteins. Science 252, 965–969.
Sakata, Y., Masuyama, T., Yamamoto, K., Nishikawa, N., Yamamoto, H., Kondo, H., Ono, K., Otsu, K., Kuzuya, T., Miwa, T., Takeda, H., Miyamoto, E., Hori, M., 2000. Calcineurin inhibitor attenuates left ventricular hypertrophy, leading to prevention of heart failure in hypertensive rats. Circulation 102, 2269–2275.
Thomas, R.R., Khan, S.M., Portell, F.R., Smigrodzki, R.M., Bennett Jr., J.P., 2011. Recombinant human mitochondrial transcription factor A stimulates mitochondrial biogenesis and ATP synthesis, improves motor function after MPTP, reduces oxidative stress and increases survival after endotoxin. Mitochondrion 11, 108–118.
Tsutsumi, T., Ide, T., Yamato, M., Kudou, W., Andou, M., Hirooka, Y., Utsumi, H., Tsutsui, H., Sunagawa, K., 2008. Modulation of the myocardial redox state by vagal nerve stimulation after experimental myocardial infarction. Cardiovasc. Res. 77, 713–721.
van Rooij, E., Doevendans, P.A., Crijns, H.J., Heeneman, S., Lips, D.J., van Bilsen, M., Williams, R.S., Olson, E.N., Bassel-Duby, R., Rothermel, B.A., De Windt, L.J., 2004. MCIP1 overexpression suppresses left ventricular remodeling and sustains cardiac function after myocardial infarction. Circ. Res. 94, e18–e26.
Vega, R.B., Rothermel, B.A., Weinheimer, C.J., Kovacs, A., Naseem, R.H., Bassel-Duby, R., Williams, R.S., Olson, E.N., 2003. Dual roles of modulatory calcineurin-interacting protein 1 in cardiac hypertrophy. Proc. Natl. Acad. Sci. U. S. A. 100, 669–674.
Wang, J., Wilhelmsson, H., Graff, C., Li, H., Oldfors, A., Rustin, P., Bruning, J.C., Kahn, C.R., Clayton, D.A., Barsh, G.S., Thoren, P., Larsson, N.G., 1999. Dilated cardiomyopathy and atrioventricular conduction blocks induced by heart-specific inactivation of mitochondrial DNA gene expression. Nat. Genet. 21, 133–137.
Wilkins, B.J., Dai, Y.S., Bueno, O.F., Parsons, S.A., Xu, J., Plank, D.M., Jones, F., Kimball, T.R., Molkentin, J.D., 2004. Calcineurin/NFAT coupling participates in pathological, but not physiological, cardiac hypertrophy. Circ. Res. 94, 110–118.

Circulation Journal
Official Journal of the Japanese Circulation Society
http://www.j-circ.or.jp

ORIGINAL ARTICLE
Hypertension and Circulatory Control

Combination Therapy of Atorvastatin and Amlodipine Inhibits Sympathetic Nervous System Activation and Improves Cognitive Function in Hypertensive Rats

Takuya Kishi, MD, PhD; Kenji Sunagawa, MD, PhD

Background: A previous study has demonstrated that orally administered atorvastatin reduces sympathetic nervous system (SNS) activation via an anti-oxidant in the rostral ventrolateral medulla (RVLM) of hypertensive rats, whereas amlodipine did not. Furthermore, several previous reports have suggested that atorvastatin or amlodipine improves cognitive dysfunction during hypertension. The aim of the present study was to determine whether a combination of atorvastatin and amlodipine causes sympathoinhibition via reduction of oxidative stress in the RVLM and improves cognitive dysfunction of hypertensive rats.

Methods and Results: Stroke-prone spontaneously hypertensive rats (SHRSPs), as a hypertensive model with sympathoexcitation, were divided into 4 groups; a combination of atorvastatin and amlodipine-treated (COM), atorvastatin-treated (ATR), amlodipine-treated (AML), hydralazine-treated (HYD), and vehicle-treated SHRSPs (VEH). After treatment for 28 days, the mean blood pressure did not change in ATR rats, and was reduced to the similar levels in COM, AML, and HYD rats. However, SNS activation and oxidative stress in the RVLM were significantly lower only in COM than in ATR, AML, HYD, and VEH rats. Cognitive performance and manganese-superoxide dismutase activity in the hippocampus were significantly higher, and oxidative stress in the hippocampus was significantly lower in COM than in VEH, AML, and HYD rats to a greater extent than in ATR rats.

Conclusions: A combination of atorvastatin and amlodipine causes sympathoinhibition via an anti-oxidant in the RVLM and improves cognitive dysfunction via an anti-oxidant in the hippocampus in hypertensive rats, independent of the blood pressure-lowering effect. (*Circ J* 2012; **76:** 1934–1941)

Key Words: Brain; Calcium channel blocker; Hypertension; Statin; Sympathetic nervous system

Hypertension and dyslipidemia can act multiplicatively or synergistically to increase the risk of a cardiovascular disease event.[1,2] Many evidences have demonstrated advantages of combined vs. older sequential and individual approaches to the treatments for hypertension and dyslipidemia.[3–5] Amlodipine is a long-acting dihydropyridine calcium channel blocker indicated for the treatment of hypertension, and previous clinical trials have suggested that amlodipine reduces cardiovascular events in different patient populations.[6–8] Atorvastatin is a 3-hydroxy-3-methylglutaryl coenzyme A reductase inhibitor (statin) indicated for the treatment of dyslipidemia and the prevention of cardiovascular disease.[4,5,9] The combination of atorvastatin and amlodipine emerged to be even more effective than each single drug alone in reducing blood pressure and in improving the lipid profile.[4,10–13]

In the development and progression in hypertension, sympathetic nervous system (SNS) activation is a main cause, and might play an additional pathophysiological role in the development of cardiovascular complications.[14,15] SNS activation is mainly regulated by the brain,[16,17] and in hypertension and heart failure models of rats, we have demonstrated that interventions to the brain have beneficial effects through sympathoinhibition.[18–27] Especially in the brain, SNS activation is mainly regulated by the rostral ventrolateral medulla (RVLM) in the brainstem, and the functional integrity of the RVLM is essential for the maintenance of basal vasomotor tone.[16,17] We have demonstrated that oxidative stress produced by an angiotensin II type 1 receptor and nicotinamide adenine dinucleotide phosphate [NAD (P) H] oxidase in the RVLM increases, and nitric oxide in the RVLM decreases the SNS activation, and that oxidative stress and nitric oxide in the RVLM have the potential to be the target of the treatments for hypertension.[18,20,22,24] Statins have been shown to reduce renal sympathetic nerve traffic, and the effect on nitric oxide and oxidative stress in the

Received March 2, 2012; revised manuscript received April 5, 2012; accepted April 6, 2012; released online May 11, 2012
Time for primary review: 23 days

Department of Advanced Therapeutics for Cardiovascular Diseases (T.K.), Department of Cardiovascular Medicine (K.S.), Kyushu University Graduate School of Medical Sciences, Fukuoka, Japan
Mailing address: Takuya Kishi, MD, PhD, Department of Advanced Therapeutics for Cardiovascular Diseases, Kyushu University Graduate School of Medical Sciences, 3-1-1 Maidashi, Higashi-ku, Fukuoka 812-8582, Japan. E-mail: tkishi@cardiol.med.kyushu-u.ac.jp

ISSN-1346-9843 doi:10.1253/circj.CJ-12-0276

brain has been proposed as possible explanations.[28] Our previous reports also suggested that orally administered atorvastatin[21,23,29] or amlodipine[19] inhibits the SNS activation via an antioxidant and/or upregulation of nitric oxide synthase in the RVLM and the brainstem of hypertensive rats. In human, several reports also have indicated the sympathoinhibitory effect of atorvastatin in hypertension.[30–32] It has not been determined, however, whether a combination of atorvastatin and amlodipine has a sympathoinhibitory effect via the reduction of oxidative stress in the RVLM of hypertensive rats.

One of the important hypertensive organ damages is cognitive dysfunction. Both hypertension and dyslipidemia are the risk factors of cognitive dysfunction,[33,34] and previous reports have suggested that atorvastatin[35] and amlodipine[36] improve cognitive dysfunction. Oxidative stress and/or antioxidant deficiency cause cognitive decline,[37] and oxidative stress in the hippocampus impairs cognitive function.[38] These previous studies indicate that each of atorvastatin or amlodipine might have a possible preventive effect on cognitive dysfunction via reduction of oxidative stress in the hippocampus. However, it has not been determined whether a combination of atorvastatin and amlodipine has a beneficial effect on cognitive dysfunction of hypertensive rats.

The aims of the present study were to investigate whether the combination of atorvastatin and amlodipine has the sympathoinhibitory effect and improvement of cognitive dysfunction in hypertensive rats. We divided stroke-prone spontaneously hypertensive rats (SHRSPs), as hypertensive and vascular dementia model rats with severe sympathetic hyperactivity,[39] into 5 groups: single atorvastatin-treatment group (ATR), single amlodipine-treatment group (AML), a combination of atorvastatin and amlodipine-treatment group (COM), hydralazine-treatment group (HYD), and vehicle group (VEH). We determined the SNS activation by 24-h urinary norepinephrine excretion, and the oxidative stress in the RVLM and hippocampus by thiobarbituric acid-reactive substances (TBARS) methods. Cognitive function was assessed by the Morris water maze test, which has been widely used as a test of spatial memory and cognition.[40]

Methods

Animals

This study was reviewed and approved by the committee on ethics of Animal Experiments, Kyushu University Graduate School of Medical Sciences, and conducted according to the Guidelines for Animal Experiments of Kyushu University. Male SHRSPs (12–14 weeks old), weighing 350–425 g were fed a standard feed (SLC Japan, Hamamatsu, Japan). They were housed individually in a temperature-controlled room (22–23°C) with a 12-h light-dark cycle (lights on at 07:00 h). We divided the SHRSPs into 5 groups: ATR, AML, COM, HYD, and VEH (n=5 for each).

Oral Administration of Amlodipine, Atorvastatin or Hydralazine

SHRSPs were treated for 4 weeks. ATR was administered atorvastatin (20 mg·kg^{-1}·day^{-1}, supplied from Pfizer Inc, New York, NY, USA). AML was administered amlodipine (5 mg·kg^{-1}·day^{-1}, supplied from Pfizer Inc, New York, NY, USA). COM was administered atorvastatin (20 mg·kg^{-1}·day^{-1}) plus amlodipine (5 mg·kg^{-1}·day^{-1}). HYD was administered hydralazine (5 mg·kg^{-1}·day^{-1}, Sigma Aldorich, St. Louis, MO, USA). VEH was administered 0.5% methylcellulose. All drugs were dissolved in 0.5% methylcellulose and administered by gastric gavage every day.

Measurement of Blood Pressure, Heart Rate and Urinary Norepinephrine Excretion

The mean blood pressure and heart rate were measured using the radio-telemetry system in rats in conscious state, every day as described previously.[22,24] At 4 weeks, we calculated the urinary norepinephrine excretion for 24 h as an indicator of the SNS activation, as described previously.[22,24]

Measurement of TBARS in the RVLM and Hippocampus

To obtain the RVLM and hippocampus tissues, the rats were deeply anesthetized with sodium pentobarbital (100 mg/kg IP) and perfused transcardially with PBS (150 mol/L NaCl, 3 mmol/L KCl, and 5 nmol/L phosphate; pH 7.4, 4°C). Prior to the removal of the brain, we made an incision on the dorsal surface of the head, and opened the bone of the head in a stereotaxic frame. RVLM was identified by the microinjected L-glutamate-induced significant and rapidly pressor response, as described previously,[18,22–25,27] and we microinjected dye into the same site. We also microinjected dye into the hippocampus according to the rat brain atlas. After these procedures, the brains were removed quickly, and 1 mm thick slices of the dye-stained tissues from the RVLM or hippocampus were obtained by using the punch-out technique with a cryostat at –7±1°C. The tissues were homogenized in 1.15% KCl (pH 7.4) and 0.4% sodium dodecyl sulfate, 7.5% acetic acid adjusted to pH 3.5 with NaOH. Thiobarbituric acid (0.3%) was added to the homogenate, and the absorbance of the organic phase was measured at 532 nm. The amount of TBARS was determined by absorbance, as described previously.[22,24]

NAD (P) H Oxidase Activity

NAD (P) H-dependent superoxide production in the RVLM and hippocampus was measured using a lucigenin luminescence assay, as described previously.[24,27] A 10% (W/vol) RVLM or hippocampus tissue homogenate was homogenized in 50 mmol/L of phosphate buffer and a luminescence assay was performed with a luminescence reader (Berthold Technology). Quantification of NAD (P) H oxidase activity was expressed relative to that in VEH, which was assigned a value of 1.

Superoxide Dismutase Activity in the RVLM and Hippocampus

Cu/Zn-superoxide dismutase (SOD) and Mn-SOD activity in the RVLM and hippocampus were assayed by monitoring the inhibition of the rate of xanthine-mediated/xanthin oxidase-mediated reduction of cytochrome *c* (pH 7.4), as described previously.[24,27] For discrimination between Cu/Zn-SOD and Mn-SOD activities, the assay was additionally performed after incubation in the presence of KCN, which selectively inhibits the Cu/Zn-SOD isoform. SOD activity was expressed relative to that in VEH, which was assigned a value of 1.

Analysis of Cognitive Function

Spatial leaning and memory function of the rats were investigated with the Morris water maze test in a circular pool filled with water at a temperature of 25.0±1°C.[40,41] In the hidden platform test, a transparent platform was submerged 1 cm below the water level. All the procedures of the Morris water maze were performed for 7 days. A pre-training session was carried out at day 0, in which animals were given 60 s free swimming without the platform. In the hidden-platform test for 4 days, the rats were given 2 trials (1 session) on day 1 and 4 trials (2 sessions) per day on days 2, 3, and 4. After mounting the plat-

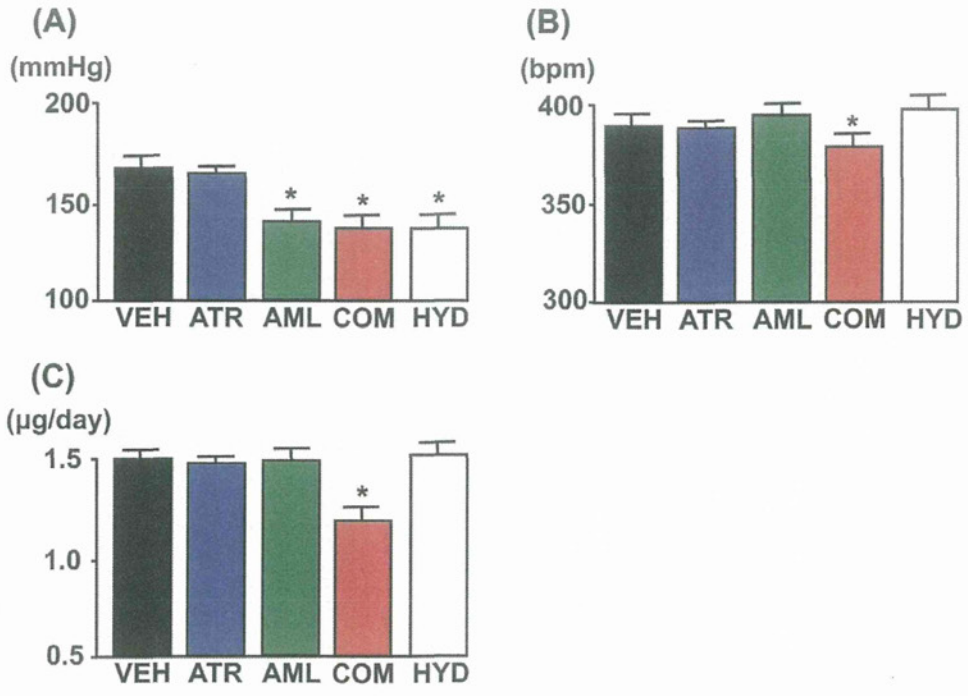

Figure 1. (A) Mean blood pressure of each group (n=5 for each). (B) Heart rate of each group (n=5 for each). (C) The 24-h urinary norepinephrine excretion of each group (n=5 for each). VEH, vehicle; ATR, atorvastatin; AML, amlodipine; COM, combination of atorvastatin and amlodipine; HYD, hydralazine. *P<0.05 vs. VEH.

form, the rats were allowed to remain there for 15 s. If a rat was unable to find the platform within 60 s, it was guided to the platform and allowed to rest on the platform for 15 s. Probe trials were performed on day 5. In the probe trial, the hidden platform was removed and the rats was released from the right quadrant and allowed to swim freely for 60 s. The time spent in the target quadrant, where the platform has been located during training, and the time spent in the other quadrants were measured. In the visible-platform test performed on day 6, the platform was elevated above the water surface and placed in a different position. The rats were given an inter-trial interval of 10 min for these trials.

Statistical Analysis

All values are expressed as mean±SEM. Comparisons between any 2 mean values were performed using Bonferroni's correction for multiple comparisons. An ANOVA was used to compare all the parameters in all groups. Differences were considered to be statistically significant at a P value of <0.05.

Results

Blood Pressure, Heart Rate, and Urinary Norepinephrine Excretion

The mean blood pressure was reduced in AML, COM, and HYD rats to similar levels, and were significantly lower in AML, COM, and HYD rats than in VEH rats (Figure 1A). The mean blood pressure was not different between ATR and VEH rats (Figure 1A). The heart rate was significantly lower in COM than in ATR, AML, HYD, and VEH rats (Figure 1B), and was not different between ATR, AML, HYD, and VEH rats. Urinary norepinephrine excretion was significantly lower in COM rats than in VEH rats, and was not different between ATR, AML, HYD, and VEH rats (Figure 1C).

TBARS Levels and NAD (P) H Oxidase Activity in the RVLM and Hippocampus

In the RVLM, TBARS levels (Figure 2A) and NAD (P) H oxidase activity (Figure 2B) were significantly lower only in COM rats than in VEH rats, and were not different between ATR, AML, HYD, and VEH rats.

In the hippocampus, TBARS levels (Figure 2C) were significantly lower in COM rats than in AML, HYD, and VEH rats to a greater extent than in ATR rats (Figure 2C). NAD (P) H oxidase activity was not different between ATR, AML, COM, HYD, and VEH rats (Figure 2D).

SOD Activity in the RVLM and Hippocampus

In the RVLM, Cu/Zn-SOD activity was not different between in COM, ATR, AML, HYD, and VEH rats (Figure 3A). However, Mn-SOD activity was significantly higher only in COM rats than in VEH rats, and was not different between ATR, AML, HYD, and VEH rats (Figure 3B).

In the hippocampus, Cu/Zn-SOD activity was not different between in COM, ATR, AML, HYD, and VEH rats (Figure 3C). Mn-SOD activity was significantly higher in COM rats than in AML, HYD, and VEH rats to a greater extent than in ATR rats (Figure 3D).

Morris Water Maze Test

In the hidden platform test, the escape latency was significantly lower in ATR rats than in AML, HYD, and VEH rats, and the performance was significantly improved in COM rats to a greater extent than in ATR rats (Figure 4A). In the probe